

Destruction of antinodal state coherence via ‘checkerboard’ charge ordering in strongly underdoped superconducting $\text{Bi}_2\text{Sr}_2\text{CaCu}_2\text{O}_{8+\delta}$

K. McElroy,^{1,2,3} D.-H. Lee,^{1,2} J. E. Hoffman,⁴ K. M. Lang,⁵ J. Lee,³ E. W. Hudson,⁶ H. Eisaki,⁷ S. Uchida,⁸ and J.C. Davis^{3,*}

¹*Physics Department, University of California, Berkeley, CA 94720 USA*

²*Material Sciences Division, Lawrence Berkeley National Lab., Berkeley, CA 94720 USA*

³*LASSP, Department of Physics, Cornell University, Ithaca, NY 14850 USA*

⁴*Department of Applied Physics, Stanford University, Stanford, CA 94305, USA*

⁵*Department of Physics, Colorado College, CO 80903, USA*

⁶*Department of Physics, MIT, Cambridge MA 02139, USA*

⁷*AIST, 1-1-1 Central 2, Umezono, Tsukuba, Ibaraki, 305-8568 Japan*

⁸*Department of Physics, University of Tokyo, Tokyo, 113-8656 Japan*

(Dated: June 21, 2004)

The doping dependence of nanoscale electronic structure in superconducting $\text{Bi}_2\text{Sr}_2\text{CaCu}_2\text{O}_{8+\delta}$ is studied by Scanning Tunneling Microscopy (STM). At all dopings, the low energy density-of-states modulations are analyzed according to a simple model of quasiparticle interference and found to be consistent with Fermi-arc superconductivity. The superconducting coherence-peaks, ubiquitous in near-optimal tunneling spectra, are destroyed with strong underdoping and a new spectral type appears. Exclusively in regions exhibiting this new spectrum, we find local ‘checkerboard’ charge-order with wavevector $\vec{Q} = (\pm 2\pi/4.5a_0, 0); (0, \pm 2\pi/4.5a_0) \pm 15\%$. Surprisingly, this order coexists harmoniously with the the low energy Bogoliubov quasiparticle states.

How the electronic structure evolves with doping from a Mott insulator into a d-wave superconductor is the key issue in understanding the cuprate phase diagram. Recently it has become clear that states in different parts of momentum space exhibit quite different doping dependences. The Fermi-arc[1] (near nodal) states of superconducting cuprates retain their coherence as doping is reduced, while the antinodal (at the edge of the 1st Brillouin zone) states diminish in coherence, eventually becoming completely incoherent at strong underdoping. Photoemission (ARPES) reveals this directly because the nodal states persist almost into the insulator[2, 3] while the antinodal states rapidly become incoherent[4–8]. Bulk probes like thermal conductivity[9] and c-axis penetration depth[10] also show that Fermi-arc states survive down to the lowest superconducting dopings. Other probes such as optical transient grating spectroscopy[11], Raman scattering[12], and NMR[13] show very different scattering processes of antinodal versus nodal states throughout the underdoped regime.

Although there is now agreement on the robust nature of the Fermi-arc states upon underdoping, a variety of different mechanisms have been proposed to account for the destruction of the antinodal coherence. These include strong scattering by both antiferromagnetic spin fluctuations[10, 13] and between the almost parallel segments of the Fermi surface near the zone face.[8, 14]

Here we report on doping-dependent STM studies of $\text{Bi}_2\text{Sr}_2\text{CaCu}_2\text{O}_{8+\delta}$ (Bi-2212) to illuminate the mechanism of antinodal decoherence. The local density of states (*LDOS*) is mapped by measuring the STM tip-sample differential tunneling conductance $g(\vec{r}, V) \equiv \frac{dI}{dV}|_{\vec{r}, V}$ at each location \vec{r} and bias voltage V . Since $LDOS(\vec{r}, E =$

$eV) \propto g(\vec{r}, V)$, an energy-resolved \vec{r} -space electronic structure map is attained. The magnitude of the energy-gap Δ , defined as half the energy difference between the coherence peaks, can also be mapped (gapmap).[15]

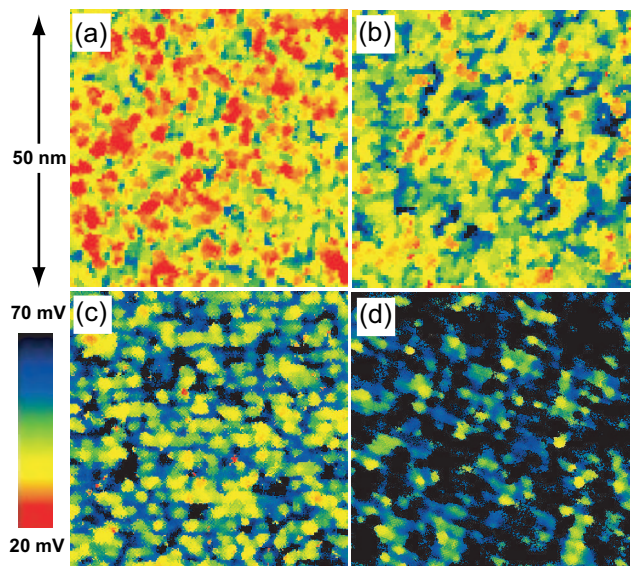


FIG. 1: (a)-(d) Measured $\Delta(\vec{r})$, gapmaps, for four different hole-doping levels as listed in I.

Fourier transform scanning tunneling spectroscopy (FT-STs) was recently introduced to cuprate studies.[16–20] It allows the \vec{q} -vectors of spatial modulations in $g(\vec{r}, V)$ to be determined from the locations of peaks in $g(\vec{q}, V)$, the Fourier transform magnitude of $g(\vec{r}, V)$. This technique has the unique capability to relate the nanoscale \vec{r} -space electronic structure to that in \vec{k} -

TABLE I: The various sample doping and average properties reported here.

Fig. 1	T_c	p (%)	$\bar{\Delta}$ (meV)	σ (meV)	P_1	P_6
(a)	89K OD	19 ± 1	33 ± 1	7	30%	0%
(b)	79K UD	15 ± 1	43 ± 1	9	5%	1%
(c)	75K UD	13 ± 1	48 ± 1	10	1%	8%
(d)	65K UD	11 ± 1	> 62	unclear	0%	$> 55\%$

space.[17]

For this study we used single Bi-2212 crystals grown by the floating zone method with the doping controlled by oxygen depletion. The samples were cleaved in cryogenic ultra-high vacuum before immediate insertion into the STM. We acquired more than 10^6 spectra for this study.

In Figure 1 we show 50 nm square gapmaps measured on samples with four different dopings. Identical color scales representing $20 \text{ meV} < \Delta(\vec{r}) < 70 \text{ meV}$ are used. The local hole concentration is impossible to determine directly, but we estimate the bulk dopings in Table I. Above optimal doping (Figure 1(a)) the vast majority of tunneling spectra are consistent with those of a $d_{x^2-y^2}$ superconductor (see Fig 2(a)). However, at the lowest dopings and for gap values exceeding $\sim 65 \text{ meV}$, there are many spectra where Δ is ill defined because no peaks exist at the gap edge (e.g. Figure 2(a), spectrum 6). We represent these spectra by black in gapmaps. The spatially averaged value of $\Delta(\vec{r})$, $\bar{\Delta}$, and its full width at half maximum, σ , are also in Table I. As doping is reduced, $\bar{\Delta}$ grows steadily consistent with other spectroscopic techniques, such as ARPES,[22] break-junction tunneling,[23] and thermal conductivity[9] which average over many nanoscale regions.

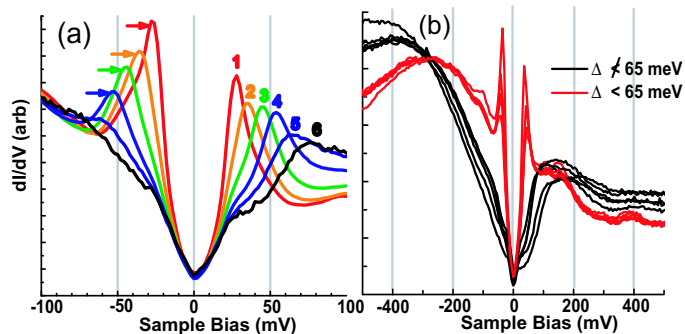


FIG. 2: (a) The average spectrum, $g(E)$, associated with each gap value in a given FOV from 1. These were extracted from 1(b) but the equivalent analysis for $g(\vec{r}, V)$ at all dopings yields results which are indistinguishable. The coherence peaks can be detected in spectra 1-4. (b) Characteristic spectra from the two regions $\Delta < 65$ (red) and $\Delta > 65$ (black)

In Figure 2(a) we show the average spectrum of all regions exhibiting a given local gap value. They are color-

coded so that each gap-averaged spectrum can be associated with regions of the same color in all gapmaps (Figure 1(a)-(d)). This set of gap-averaged spectra is almost identical for all dopings. The changes with doping seen in $\Delta(\vec{r})$ occur because the probability of observing a given type of spectrum (1-6) in Fig 2(a) evolves rapidly with doping (Table I).

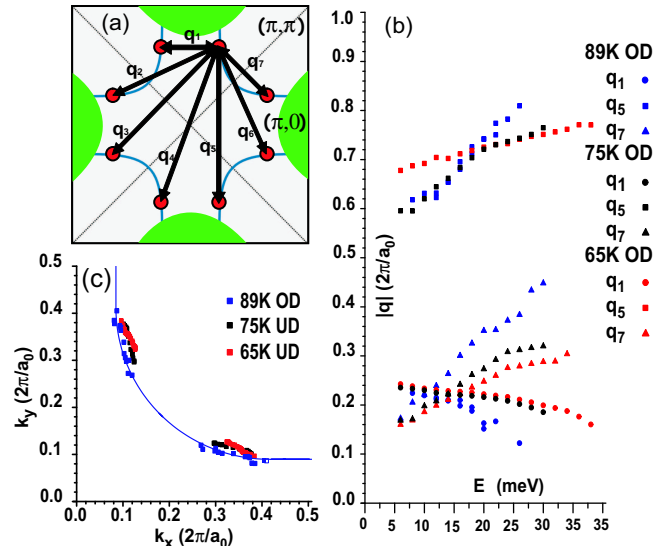


FIG. 3: (a) A schematic representation of the 1st Brillouin zone and Fermi arc location of Bi-2212. The flat-band regions near the zone face are shaded in green. The eight locations which determine the scattering within the ‘octet’ model[17] (for one sub gap energy) are shown as red circles and the scattering vectors which connect these locations are shown as arrows labelled by the designation of each scattering vector. (b) Measured dispersions of the LDOS-modulations \vec{q}_1 , \vec{q}_5 and \vec{q}_7 for the 3 dopings whose gapmaps are shown in Fig 1 (a), (c), and (d). (c). Calculated loci of scattering, \vec{k}_s for all 3 dopings.

Despite the intense changes with doping in the gapmaps, the $LDOS$ at energies below about $0.5\bar{\Delta}$ remains relatively homogenous for all dopings studied [Figure 2(a)]. These low energy $LDOS$ do, however, exhibit numerous weak, incommensurate, energy-dispersive, $LDOS$ -modulations with long correlation lengths [16–18, 20]. To explore the doping dependence of these low energy $g(\vec{r}, V)$ we use the FT-STs technique and the ‘octet’ model.[17, 21] Figure 3(b) (using the \vec{q} -vector designations in Figure 3(a)) shows the measured length of \vec{q}_1 , \vec{q}_5 and \vec{q}_7 as a function of energy for the three data sets. Figure 3(c) shows the locus of scattering $\vec{k}_s(E)$ [17] calculated for these three $g(\vec{r}, V)$. These $\vec{k}_s(E)$ differ only slightly between dopings and are the same for filled and empty states.

The doping dependence of states with $\vec{k} \approx (\pm\pi/a_0, 0), (0, \pm\pi/a_0)$ in the ‘flat band’ region near the zone-face (green shaded in Fig 2(a)) is extremely different. By definition, the coherence peaks in $g(\vec{r}, V)$ occur at $E = \Delta(\vec{r})$. In all samples, they exhibit

intense bias symmetric intensity modulations in the *LDOS*, with wavevectors $\vec{G} = (\pm 2\pi/a_0, 0), (0, \pm 2\pi/a_0)$. These coherence-peak *LDOS*-modulations at $\vec{q} = \vec{G}$ seem to be from Umklapp scattering between $\vec{k} \approx (\pm\pi/a_0, 0), (0, \pm\pi/a_0)$. [17] Therefore, the coherence-peaks in tunneling are identified empirically with the zone-face states at $\vec{k} \approx (\pm\pi/a_0, 0), (0, \pm\pi/a_0)$, consistent with theory. We therefore consider any spatial regions that show clear coherence-peaks plus $\vec{q} = \vec{G}$ *LDOS*-modulations to be occupied by a canonical d-wave superconductor (dSC).

Near optimal doping, more than 98% of any FOV exhibits this type of coherence-peaked spectrum. As the range of local values of $\Delta(\vec{r})$ increases with decreasing doping, the intensity of the $\vec{q} = \vec{G}$ coherence-peak *LDOS*-modulations becomes steadily weaker until, wherever $\Delta(\vec{r}) \not\prec 65$ meV, they disappear altogether. This process can be seen clearly in the gap-averaged spectra of Fig 2(a). Wherever the coherence-peaks and associated $\vec{q} = \vec{G}$ *LDOS*-modulations are absent, a well-defined new type of spectrum is always observed. Examples of this new type of spectrum, along with those of coherence-peaked dSC spectra, are shown in Fig 2(b). The coherence-peaked spectra (red) are manifestly distinct from the novel spectra (black) which have a V-shaped gap reaching up to ± 75 meV but with very different evolutions at opposite bias beyond these energies. For reasons to be discussed below, we refer to the new spectrum (black in Fig 2 (b)) as the zero temperature pseudogap (ZTPG) spectrum.

The replacement of coherence-peaked spectra by ZTPG spectra first begins to have strong impact on averaged properties of $g(\vec{r}, V)$ and $g(\vec{q}, V)$ below about $p = 0.13$ where the fractional area covered by ZTPG spectra first exceeds $\approx 10\%$ of the FOV. No further evolution in spectral shape of the ZTPG spectrum is detected at lower dopings. Instead, a steadily increasing fractional coverage of the surface by these ZTPG spectra is observed. Our previous studies [15–17] were carried out at dopings $p > 0.13$ where ZTPG spectra comprise a tiny fraction of any FOV. Significantly, spectra similar to the ZTPG spectrum are detected inside vortex cores of Bi-2212 where superconductivity is destroyed. [24, 25] Furthermore, a very similar spectrum is observed in another very underdoped cuprate $\text{Na}_x\text{Ca}_{2-x}\text{CuO}_2\text{Cl}_2$, even in the non-superconducting phase. [26] It therefore seems reasonable that this spectrum is characteristic of the electronic phase that exists at zero-temperature in the pseudogap (ZTPG).

Next we introduce a masking process illuminate the electronic structure of ZTPG nano-regions. From a given strongly underdoped data set (Fig 1 (d)), the $g(\vec{r}, V)$ in all regions where $\Delta(\vec{r}) \not\prec 65$ meV are excised and used to form a new masked data set $g(\vec{r}, V)|_{\Delta \not\prec 65}$. The remainder forms a second new data set $g(\vec{r}, V)|_{\Delta < 65}$. The cutoff

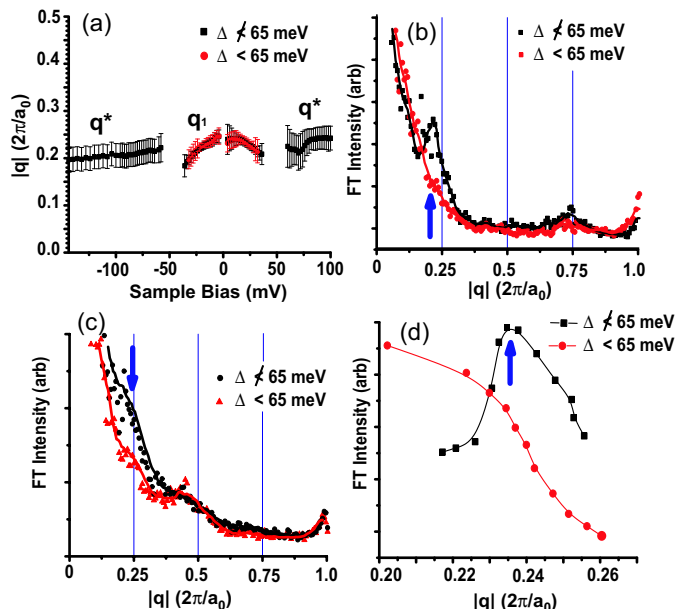


FIG. 4: (a) Dispersion of \vec{q}_1 in regions with dSC coherence-peaked spectra $\Delta < 65$ meV (red circles). Dispersion of in regions with ZTPG spectra for $E < 36$ meV (black squares). For $E > 65$ meV, the wavevector of the \vec{q}^* new modulations in ZTPG regions are shown in black. To within our uncertainty they do not disperse and exhibit $\vec{q}^* = (\pm 2\pi/4.5a_0, 0), (0, \pm 2\pi/4.5a_0) \pm 15\%$. (b) The magnitude of the $g(\vec{q}, V)$ integrated between -65 meV and $+150$ meV along the \vec{q}_1 direction for $\Delta \not\prec 65$ meV ($\Delta < 65$ meV) black (red). Solid lines are guides to the eye. (c) The magnitude of the Fourier transform of the masked topographic image along the \vec{q}_1 direction for $\Delta \not\prec 65$ meV and ($\Delta < 65$ meV) black (red). Solid lines are guides to the eye. (d) A plot of the amplitude of the \vec{q}_1 *LDOS*-modulation as a function of $|\vec{q}_1|$ for the same data set yielding Figures 1(d). The maximum intensity of the modulations in the ZTPG regions occurs at $|\vec{q}_1| = 2\pi/4.5a_0 \pm 10\%$. No enhanced scattering of the quasi-particles in the dSC regions (red) is seen near any \vec{q} -vector. The \vec{q} -space resolution a masked data set is far less than that in previous studies. [17]

$\Delta(\vec{r}) < 65$ meV was chosen because it represents where the coherence-peaks with $\vec{q} = \vec{G}$ associated modulations have disappeared and are replaced by the ZTPG spectra.

FT-STs analysis of such $(g(\vec{r}, V)|_{\Delta \not\prec 65}, g(\vec{r}, V)|_{\Delta < 65})$ pairs shows that they exhibit dramatically different phenomena. In the $g(\vec{r}, V)|_{\Delta < 65}$, the dispersive trajectory of \vec{q}_1 is seen up to $E \approx 36$ meV and no further *LDOS*-modulations can be detected at any higher energy (red symbols in Figure 4(b)). In the $g(\vec{r}, V)|_{\Delta \not\prec 65}$ data, the identical dispersive \vec{q}_1 signal is seen below $E \approx 36$ meV but, in addition, a new nondispersive *LDOS*-modulation appears between $E = -65$ meV and our maximum measured energy $E = -150$ meV (black symbols in Fig 4(a)) with a wavevector $\vec{q}^* = (\pm 2\pi/4.5a_0, 0), (0, \pm 2\pi/4.5a_0) \pm 15\%$.

To search for non-dispersive *LDOS* modulations inte-

gration over energy is often used.[19, 20] In Figure 4 (b) we show the Fourier transform magnitude of the both components of the masked *LDOS* integrated over the energy range where we see \vec{q}^* (from Fig 1 (d)). The ZTPG regions show a peak at the same well defined wavevector set $\vec{q}^* = (\pm 2\pi/4.5a_0, 0), (0, \pm 2\pi/4.5a_0) \pm 15\%$ while the dSC regions show no such effect.

An even more conclusive technique for detection of net charge density modulations is constant-current topography because it represents, albeit logarithmically, the contour of constant integrated density of states. We apply the identical mask ($\Delta \not\prec 65$ meV) to the topographic image acquired simultaneously with the gapmap in 1(d). The magnitude of the Fourier transform along the $\vec{q}|| (2\pi, 0)$ for this masked topographic image shows that, in the ZTPG regions, the topography is modulated with $q_{topo} = (\pm 2\pi/4.7a_0, 0), (0, \pm 2\pi/4.7a_0) \pm 20\%$ (indicated by the arrow in Fig 4(c)). No such modulations at any wavelengths near this q_{topo} are found in $\Delta < 65$ meV regions (red in Fig 4(c)).

A static charge modulation with wavevector \vec{Q} should[27–30] influence quasiparticle scattering to cause an enhancement in $g(\vec{Q}, V)$ for any V . Our measurements of the intensity of the dispersive quasi-particle branch, \vec{q}_1 , reveal a maximum in $g(\vec{q}_1, V)$ (in the ZTPG regions only) when $\vec{q}_1 = \vec{Q} = (\pm 2\pi/4.2a_0, 0), (0, \pm 2\pi/4.2a_0) \pm 15\%$ (in Fig 4(d)). This provides further evidence of charge order exclusively in ZPTG regions.[31]

These observations motivate three new insights into the electronic structure of $\text{Bi}_2\text{Sr}_2\text{CaCu}_2\text{O}_{8+\delta}$. First, quasiparticle interference occurs between states in approximately the same region of \vec{k} -space for all dopings. These Fermi-arc quasiparticles are Bogoliubov-like in the sense that they exhibit particle-hole symmetry at each location in \vec{k} -space and are consistent with one $\Delta(\vec{k})$ for each doping. Therefore, the Fermi-arc states are robust and gapped by superconductivity at all dopings studied.

Our second finding is the very different fate of states in the flat-band regions near $\vec{k} \approx (\pm\pi/a_0, 0)(0, \pm\pi/a_0)$. The appearance of ZTPG spectra in strongly underdoped samples coincides with the destruction of antinodal superconducting coherence-peaks. Exclusively in these ZTPG regions, which only occur in strongly underdoped Bi-2212, multiple independent phenomena with the same wavevector $\vec{Q} = \vec{q}_{topo} = \vec{q}^* = (\pm 2\pi/4.5a_0, 0), (0, \pm 2\pi/4.5a_0) \pm 15\%$ point to the appearance of an unusual charge ordered state. We refer to this as a ‘checkerboard’ state because Fourier analysis of all these phenomena shows that they are symmetric under 90 rotations.

The third point is that the low energy quasiparticle interference effects indicate the existence of Bogoliubov quasiparticles in *both* the ZTPG and dSC regions.

Consistent with previous deductions[1–13], we therefore find two distinct regions of \vec{k} -space; the Fermi-

arc supporting robust coherent quasiparticle states, and the antinodal region gapped by superconductivity at higher doping but becoming progressively incoherent below $p \sim 0.13$. But here we demonstrate for the first time that antinodal decoherence is closely related to the emergence of the ‘checkerboard’ charge order. Furthermore, we find that this order is not mutually exclusive with the Bogoliubov Fermi-arc states, but rather they coexist throughout the sample. This miscibility between the low energy excitations of a high T_c superconductor and the charge ordered state has strong implications for the phase diagram. It also provides severe constraints on microscopic theories of strongly underdoped cuprate electronic structure.

We acknowledge and thank A. V. Balatsky, S. Chakravarty, M. P. A. Fisher, T. Hanaguri, N. E. Hussey, S. Kivelson, P. A. Lee, A. Millis, D. Pines, S. Sachdev, J. Sethna, T. Uemura, A. Yazdani, J. Zaanen, and S.-C. Zhang for very helpful discussions and communications.

* jcdavis@ccmr.cornell.edu

- [1] M. R. Norman *et al.*, *Nature* **392**, 157 (1998).
- [2] T. Yoshida *et al.*, *Phys. Rev. Lett.* **91**, 027001 (2002).
- [3] F. Ronning *et al.*, *Phys. Rev. B* **67**, 165101 (2003).
- [4] A. G. Loeser *et al.*, *Phys. Rev. B* **56**, 14185 (1997).
- [5] A. V. Fedorov *et al.*, *Phys. Rev. Lett.* **82**, 2179 (1999).
- [6] D. L. Feng *et al.*, *Science* **289**, 277 (2000).
- [7] H. Ding *et al.*, *Phys. Rev. Lett.* **87**, 227001 (2001).
- [8] X. J. Zhou *et al.*, *Phys. Rev. Lett.* **92**, 187001 (2004).
- [9] M. Sutherland *et al.*, *cond-mat/0301105*.
- [10] A. Hosseini *et al.*, *cond-mat/0312542*.
- [11] N. Gedik *et al.*, *Science* **30**, 1410 (2003).
- [12] Y. Gallais, A. Sacuto, T. P. Devereaux, and D. Colson, *cond-mat/0403753*.
- [13] D. Pines, *cond-mat/0404151*.
- [14] H. C. Fu, J. C. Davis, and D.-H. Lee, *cond-mat/0403001*.
- [15] K. M. Lang *et al.*, *Nature* **415**, 412 (2002).
- [16] J. E. Hoffman *et al.*, *Science* **297**, 1148 (2002).
- [17] K. McElroy *et al.*, *Nature* **422**, 592 (2003).
- [18] M. Vershinin *et al.*, *Science* **303**, 1995 (2004).
- [19] J. E. Hoffman *et al.*, *Science* **295**, 466 (2002).
- [20] C. Howald *et al.*, *Phys. Rev. B* **67**, 014533 (2003).
- [21] L. Zhu, W. A. Atkinson, and P. J. Hirschfeld, *Phys. Rev. B* **69**, 060503(R) (2004).
- [22] A. Damascelli, Z. Hussain, and Z.-X. Shen, *Rev. Mod. Phys.* **75**, 473 (2003).
- [23] N. Miyakawa *et al.*, *Phys. Rev. Lett.* **80**, 157 (1998).
- [24] Ch. Renner *et al.*, *Phys. Rev. Lett.* **80**, 3606 (1998).
- [25] S. H. Pan *et al.*, *Phys. Rev. Lett.* **85**, 1536 (2000).
- [26] T. Hanaguri *et al.*, to be published.
- [27] M. Vojta, *Phys. Rev. B* **66**, 104505 (2002).
- [28] D. Podolsky, E. Demler, K. Damle, and B. I. Halperin, *Phys. Rev. B* **67**, 094514 (2003).
- [29] C.-T. Chen and N.-C. Yeh, *Phys. Rev. B* **68**, 220505 (2003).
- [30] L. Capriotti, D. J. Scalapino, and R. D. Sedgewick, *Phys. Rev. B* **68**, 014508 (2003).
- [31] Similar phenomena have been discovered where super-

conductivity is destroyed leaving pseudogap like spectra. Incommensurate, low energy, 'checkerboard', *LDOS*-modulations are found both surrounding vortex cores[19]

and in the pseudogap phase above T_c [18]